NASA Technical Memorandum 4034

Preliminary Investigation of Stability of a Fin-Stiffened Slender Strut

Mark S. Lake and K. Chauncey Wu
Langley Research Center
Hampton, Virginia

National Aeronautics
and Space Administration

Scientific and Technical
Information Division

1988

Introduction

A major goal in designing a space structure is to ensure adequate structural performance of the assembled truss while minimizing the packaged volume of the structure for transportation to orbit (ref. 1). A fin-stiffened strut concept which addresses the difficult goal of simultaneously achieving high strut bending stiffness and low packaged volume has been identified for use on large space structures.

The fin-stiffened strut (fig. 1) is designed to increase truss member buckling loads and vibration frequencies by providing an increased effective cross-sectional moment of inertia with a small packaged outer diameter. The increased inertia is obtained by deploying three curved fins from a core tube. The fins are 120° sections of a right circular cylinder which has its inner diameter equal to the outer diameter of the core tube. In the undeployed position, the fins lie flush around the outside of the core tube, each being attached to the core by a hinge along one of the edges of the fin. When deployed, the fins rotate out from the core to an angle which maximizes the cross-sectional moment of inertia. Because of symmetry of this configuration, the strut cross section has the same principal moments of inertia (i.e., $I_{XX} = I_{YY}$ and $I_{XY} = 0$) for any orientation of a set of axes with origin at the centroid; and thus, the strut does not have a preferred direction of buckling or vibration.

It is necessary to understand the behavior of the fin-stiffened strut before it can be incorporated into the design of a space structure. This report describes a preliminary investigation of the structural stability of one fin-stiffened strut design. The objectives of this study are to evaluate three fin-to-core attachment concepts and to determine the finite element modeling complexity necessary to predict the fin-stiffened strut buckling load. These objectives are accomplished by comparing results from laboratory testing and finite element analyses.

Symbols

EI	flexural stiffness, lbf-in^2
I_{XX}, I_{YY}, I_{XY}	cross-sectional area moments of inertia, in^4
l	strut length, in.
L/ρ	strut slenderness ratio
P_e	Euler buckling load, lbf
P_{cr}	buckling load predicted with finite element models, lbf
ρ/t	strut radius of gyration to thickness ratio

Strut Description

A strut design having the dimensions shown in figure 2 was chosen for this study because test specimens could be easily fabricated with stock aluminum tubing. The length of this strut is 77 in., its cross-sectional area is 0.102 in^2, and figure 3 shows the variation of its cross-sectional moment of inertia with fin deployment angle. The data for figure 3 were derived from an exact solution of the double integral expression for area moment of inertia. The moment of inertia reaches a maximum when the fin deployment angle is 128°; this makes the distance between the fin centroids and the strut axis of revolution also a maximum. Since the deployed moment of inertia does not vary greatly from its maximum for deployment angles between 100° and 150°, a fin deployment angle of 150° was chosen to simplify construction of the test specimens. The cross-sectional moment of inertia for a deployment angle of 150° is 1.777×10^{-2}in^4. The value of Young's modulus for the aluminum tubing used in the test hardware is assumed to be 10.6×10^6 lbf/in^2; thus, the flexural stiffness of the strut cross section (EI_{XX} and EI_{YY}) is 1.883×10^5 lbf-in^2.

The fin-stiffened strut requires a hinge mechanism to attach the fins to the core tube. Three fin attachment concepts that exhibit the core-to-fin load transfer capability and restraint characteristics of probable hinge designs were identified for this study, and specimens representing these concepts were fabricated for testing. The first attachment concept represents a design which uses independent hinges for each of the three fins. This concept allows the fins to move independently of the core and each other in the axial direction and together in the lateral direction while inhibiting axial load transmission between the core and the fins. Independent axial motion of the fins is achieved in the test specimen (specimen 1) by welding each fin to separate collars which slide over the core tube. (See fig. 4.) The second fin attachment concept represents a design which allows the fins to move together but independently of the core in the axial direction and all components to move together in the lateral direction. This concept also inhibits the transmission of axial load between the core and the fins. In this test specimen (specimen 2), all fins are welded to common collars which slide over the core tube. (See fig. 5.) The third concept represents an ideal, rigid connection between the fins and the core. This test specimen (specimen 3) has all fins welded to the core tube. (See fig. 6.)

The Euler buckling load of a simply supported slender column is given in the following equation (ref. 2):

$$P_e = \frac{\pi^2 EI}{L^2} \qquad (1)$$

Equation (1) is derived from classical beam theory assuming an ideal, straight, prismatic beam and neglecting the effects of transverse shearing and cross-sectional warping.

Test specimen 3 is described as ideal because it is expected to behave according to the assumptions of classical beam flexure theory. Therefore the buckling load of specimen 3 can be predicted by using equation (1) and assuming the area moment of inertia determined from figure 3. Additionally, the buckling load of the core tube can be predicted by using equation (1) and assuming the area moment of inertia of the core by itself. Test specimens 1 and 2 are expected to exhibit buckling loads lower than specimen 3 because their cross sections can warp during bending and their fins are attached with no shear load transfer capability. However, the buckling load of specimen 1 can also be predicted by using equation (1) and assuming that the effective moment of inertia of the cross section is equal to the sum of the inertias of the core and the fins taken at their respective centroids. This approach is justified by considering the deformation of the specimen when acted on by lateral or bending loads. Each component (the core and the fins) must assume the same lateral deformation and must have no net axial load due to the lack of shear load transfer between the components. Therefore the bending stiffness of the specimen is equal to the sum of the bending stiffnesses of the components. The buckling load of specimen 2 should be between those of specimens 1 and 3, because the fin attachment collars on specimen 2 allow shear load transfer between the fins. The results of testing and finite element analysis of specimens 1 and 3 and the core tube can be compared with results from equation (1) for verification of the test setup and finite element models.

Testing

Stability tests were performed on the core tube and the three fin-stiffened strut specimens for two boundary conditions: pinned and partially restrained. Data from the partially restrained tests (see appendix A) indicate that there are uncertainties associated with the partial restraint support fixtures. However, the ratio of actual buckling load to ideal buckling load for the various fin attachment concepts studied is nearly the same for the pinned and partial end restraints. Therefore, due to the questionable nature of the partial end restraint data, correlation between tests and finite element analyses is only based on the pinned boundary condition data.

Test Setup

The setup used for the strut tests (fig. 7(a)) consisted of the test specimen instrumented with two lateral and one axial differential current displacement transducers (DCDT's), an upper platen supporting a load cell (fig. 7(b)), a guide assembly for the lateral DCDT's (fig. 7(c)), and a lower platen supporting both the DCDT's and a moving platform (fig. 7(d)). The axial load was applied quasi-statically by using a hand crank to translate the platform mounted on the lower platen in the strut's axial direction. The upper and lower platens were rigidly bolted to a permanent backstop. Two sets of fixtures were used to mount the specimens to the platens. The first, shown in figure 8(a), provided a pinned support for the specimen and had a center of rotation 0.875 in. from the end of the specimen. The second, shown in figure 8(b), was designed to provide a clamped restraint but only provided a partial lateral restraint due to compliance in the fit of the components.

The lateral deflections of the strut at its midspan were transmitted through monofilament line to two DCDT's located 90° apart, and a third DCDT was used to measure the axial motion between the upper platen and the translating platform on the lower platen. Two inactive DCDT's were attached opposite the active DCDT's at the midspan to balance out any lateral forces which might induce a preferred direction of strut failure (figs. 7(c) and 7(d)). Data were collected with a personal computer-based data acquisition system and analyzed with a personal computer-based spread-sheet program.

Test Results

Strut buckling loads were determined for all specimens from plots of axial load versus both axial and lateral deflections. Figure 9 is a plot of axial load versus lateral deflection for a typical test run (specimen 2, run 2). Theoretical pinned-pinned buckling loads for the core tube, specimen 1, and specimen 3 were calculated from equation (1) and compared with experimental results to validate the test setup. These theoretical buckling loads are 36.2 lbf, 59.9 lbf, and 299.7 lbf, respectively, by using the dimensions presented in figure 2 and an effective tube length of 78.75 in. (77 in. tube length plus the 0.875-in. offset in each support fixture). Experimentally determined pinned-pinned buckling loads for the core tube and the three stiffened strut specimens are presented

in table 1 along with the theoretical loads. The experimental loads for the core tube, specimen 1, and specimen 3 agree to within 8 percent of the theoretical values.

Table 1. Experimental Pinned-Pinned Buckling Loads

Specimen	Theoretical buckling load,* lbf	Buckling load, lbf, for Run 1	Buckling load, lbf, for Run 2
Core tube	36.2	39.0	37.8
1	59.9	63.3	63.1
2		224.0	220.0
3	299.7	283.0	283.0

*Derived from equation (1).

One concern about the accuracy of the experimental data is that misalignment of both the specimens within the support fixtures and the support fixtures on the platens would cause nonideal loading of the specimen and, therefore, affect the measured buckling load. Thus, two test runs were performed on each specimen to determine the sensitivity of the buckling load to the orientation of the specimen within the support fixtures. Between these runs, the specimen was rotated 90° around its longitudinal axis. If misalignment existed it would be indicated by a variation of the measured buckling load as the specimen orientation was changed. The two columns in table 1 entitled "Run 1" and "Run 2" present the results from these test runs. Agreement between these results indicates that the pinned support fixtures were adequately aligned for all the specimens.

As expected, specimen 3 exhibited the highest buckling load of the three specimens, and the load could be predicted with classical beam flexure theory. Specimen 2, which had fins that were constrained to move together axially, exhibited the next highest buckling load which was about 78 percent of the load obtained with specimen 3. Specimen 1, which had fins that could move independently in the axial direction, exhibited the lowest buckling load, having a value that was only 22 percent of the load obtained with specimen 3.

Finite Element Analysis

Finite element analyses of the three stiffened strut concepts were performed to determine the predictability of the buckling load by using this analysis technique. Two approaches to modeling the structure were examined. With the first approach, the core and fins were modeled with plate elements, and with the second approach, the core and fins were modeled with equivalent beam elements. The results from these models were compared on the bases of accuracy and computation time.

Description of Models

Finite element models of the fin-stiffened strut were developed by using the Engineering Analysis Language (EAL, ref. 3), and sections from the two types of models are compared in figure 10. The first model incorporates four node plate (membrane and bending stiffness) elements, having an aspect ratio of 3.4, to represent 30° arc segments of the core and fins. This discretization scheme was based on results from a study of the effects of element aspect ratio on solution accuracy. (See appendix B.) The second model incorporates beam elements to represent the core and fins and has approximately 85 percent fewer degrees of freedom than the plate model.

The three fin-to-core attachment concepts were modeled by using spring elements. Collars which only had one fin attached were modeled with spring elements connecting the fins to the core. These connecting elements had no stiffness in the strut axial direction and infinite stiffness in the strut radial and tangential directions, thus allowing each fin to move independently of the others in the strut axial direction. Collars to which all three fins were attached were modeled as an equilateral triangle assembly of rigid beam elements connecting the bases of the fins. These triangles were then connected to the core by using spring elements with zero stiffness in the strut axial direction. Spring elements having infinite stiffnesses in all directions were used to model the welded joint in the third fin-to-core attachment concept. Finally, the pinned support fixtures were modeled with 0.875-in-long beam elements, rigidly attached at one end to the strut and pinned at the other end to ground.

Analytical Results

The results from the finite element analyses are presented in table 2 and are compared with average values of buckling load determined for each test specimen. All the models constructed with plate elements gave results that differed by less than 10 percent from experimental results. Results from the models constructed with equivalent beam elements also differed by less than 10 percent from experimental results for all specimens except specimen 2, for which the calculated buckling load was 17.2 percent higher than that derived from experiment. The computer time required to solve the eigenvalue problem for the plate

models was 35 to 40 times longer than that required for the beam models.

Table 2. Finite Element Pinned-Pinned Buckling Loads

Specimen	Average experimental buckling load,* lbf	Buckling load, lbf, for—	
		Plate models	Beam models
Core tube	38.4	38.5 (†0.3%)	36.2 (5.7%)
1	63.2	58.0 (8.2%)	59.3 (6.2%)
2	222.0	222.6 (0.3%)	260.2 (17.2%)
3	283.0	256.5 (9.4%)	289.9 (2.4%)

*Average values from two experimental runs on each specimen.

†Percent difference from average experimental value.

Concluding Remarks

In this study, the stability of a fin-stiffened strut has been investigated and three fin attachment concepts have been compared. An ideal value, or upper bound, of the fin-stiffened strut buckling load is provided by a strut design incorporating welded fin connections. A lower bound of the strut buckling load is approximately 20 to 25 percent of the ideal value and is provided by a strut design which allows the individual fins and core to move independently in the strut axial direction. A practical strut design, incorporating hinge assemblies which constrain the fins to move together but independently of the core tube in the strut axial direction, provides a buckling load which is 75 to 80 percent of the load from the ideal design. Since the ratio of actual buckling load to ideal buckling load for the various fin attachment concepts was insensitive to the end restraint of the strut, their performance can be compared by using simple pinned boundary conditions.

Buckling loads for the bounding designs represented by specimens 1 and 3 can be accurately predicted by Euler's equation. Predicting the buckling loads for practical designs represented by specimen 2 requires more detailed analysis such as finite element analysis. Flat plate finite element models of the strut considered herein provided results that agree to within 10 percent of the experimental values for all fin attachment designs. Although the same accuracy was obtained with equivalent beam models of specimens 1 and 3, an equivalent beam model of specimen 2 provided a buckling load that was 17.2 percent higher than that derived from experiment, and thus the added detail of the plate representation appears necessary to accurately predict the performance of practical fin-stiffened strut designs. Furthermore, element aspect ratios of 3 and below must be used when constructing a flat plate finite element model of a fin-stiffened strut with arbitrary slenderness and radius of gyration to thickness ratios.

NASA Langley Research Center
Hampton, VA 23665-5225
February 22, 1988

Appendix A

Stability Tests of Fin-Stiffened Strut With Partial End Restraints

Stability tests were performed with the specimens mounted in the partial restraint fixtures using the same setup and procedures described in the accompanying report for the pinned tests. Again, two runs were made for each specimen to determine if any misalignment existed. Preliminary results showed that the fixtures were aligned for specimens 1 and 2 but misaligned for specimen 3. Specimens 1 and 2 shared the same core tube whereas specimen 3 was fabricated with its own core tube because its fins were permanently attached. All the ends of these core tubes had been bored out to accept the support fixtures. Furthermore, it was observed that the ends of specimen 3 had been poorly bored and when the support fixtures were inserted, they were visibly misaligned with the specimen. Subsequent attempts to correct the misalignment provided some improvement in the data, but, as the results in table A1 indicate, the misalignment could not be eliminated, and the buckling load measured for specimen 3 varied significantly with its orientation in the support fixture.

Table A1. Experimental Partially Restrained Buckling Loads

Specimen	Buckling load, lbf, for—	
	Run 1	Run 2
1	114.4	116.0
2	309.0	295.0
3	438.0	375.0

Although there is some uncertainty with regard to the partial restraint results for the fin attachment concepts studied, the ratio of actual buckling load to ideal buckling load was nearly the same for both pinned and partial end restraints. Therefore, the trends indicated by the partial restraint results are consistent with those seen in the pinned tests. Once again, specimen 3 had the highest buckling load, and specimens 2 and 1 had buckling loads which were approximately 75 percent and 25 percent, respectively, of the specimen 3 buckling load. To avoid the uncertainties associated with the partial restraint support fixtures, finite element analyses discussed in the main text of this report address only the pinned boundary conditions.

Appendix B

Considerations for Modeling the Fin-Stiffened Strut Using Flat Plate Elements

Preliminary stability analyses of the fin-stiffened strut using the flat plate finite element model indicated that the computed buckling loads were very sensitive to the aspect ratio of the elements making up the core tube and fins. To better understand the accuracy of the results obtained from the flat plate finite element model, a parametric study was conducted to determine the sensitivity of the computed buckling loads of the core tube to the aspect ratio of plate elements.

A series of analyses were performed by using models with 12 node points representing the circular cross sections to determine the pinned-pinned and clamped-clamped buckling loads of core tubes having a range of slenderness and radius of gyration to thickness ratios. Data from these models are presented in figures B1 and B2 and normalized to the corresponding values computed from Euler theory (P_e and $4P_e$, respectively). The data show that the buckling load derived from finite element analysis of the core tube compares well with the theoretical value when element aspect ratios are less than 3, regardless of the boundary condition or the tube slenderness and radius of gyration to thickness ratios. However, for aspect ratios greater than 3, the solution accuracy can vary greatly for both boundary conditions depending on the slenderness and radius of gyration to thickness ratios of the tubes. Based on the findings of this study, it is recommended that element aspect ratios of 3 and below be used for EAL finite element stability analyses of this type of structure with arbitrary slenderness and radius of gyration to thickness ratios. Additionally, because of the simplifying kinematic assumptions made with a flat plate representation of the structure, it may be advantageous to model struts with small radius of gyration to thickness ratios with three-dimensional solid elements.

The core tube analyzed in the accompanying report has a slenderness ratio of 495.2 and a radius of gyration to thickness ratio of 2.39. Modeling it with 12 nodal points representing the cross section and using elements with an aspect ratio of approximately 3.4 results in a computed buckling load that differs from the Euler solution by only 6 percent. Additionally, an element aspect ratio of 3.4 eases discretization of the structure by providing convenient nodal point locations for incorporating the fin attachment collars described in the main text of this report. Therefore, an element aspect ratio of approximately 3.4 was selected for all analyses presented in this report to ensure accuracy and ease discretization of the structure.

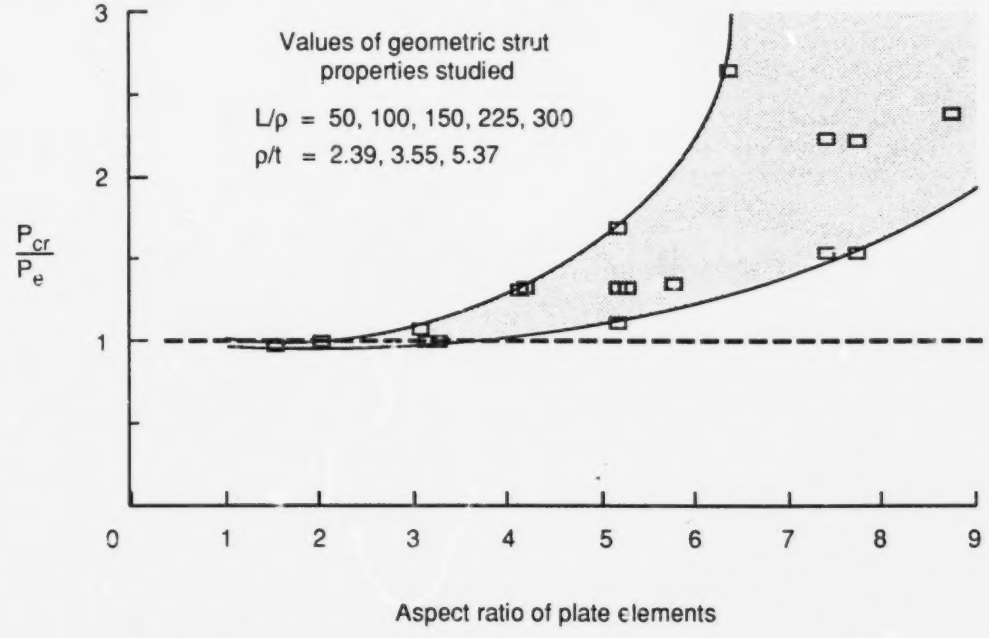

Figure B1. Pinned boundary condition parametric study results.

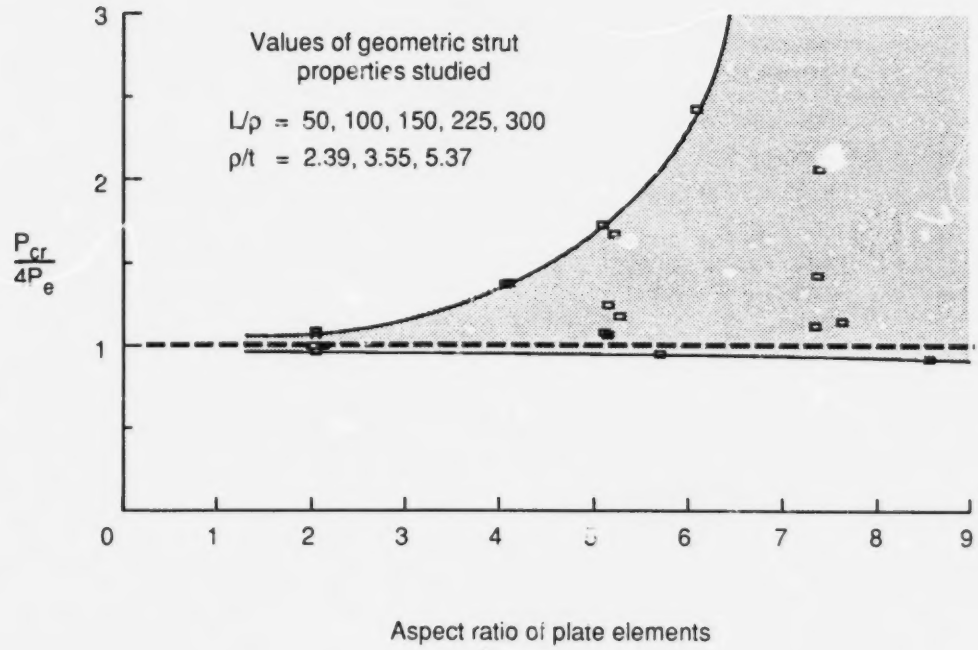

Figure B2. Clamped boundary condition parametric study results.

References

1. Mikulas, Martin M., Jr.; Croomes, Scott D.; Schneider, William; Bush, Harold G.; Nagy, Kornell; Pelischek, Timothy; Lake, Mark S.; and Wesselski, Clarence: *Space Station Truss Structures and Construction Considerations.* NASA TM-86338, 1985.
2. Timoshenko, Stephen P.; and Gere, James M.: *Theory of Elastic Stability.* Second ed. McGraw-Hill Book Co., 1961.
3. Whetstone, W. D.: *EISI-EAL Engineering Analysis Language Reference Manual EISI-EAL System Level 2091.* Engineering Information Systems, Inc., July 1983.

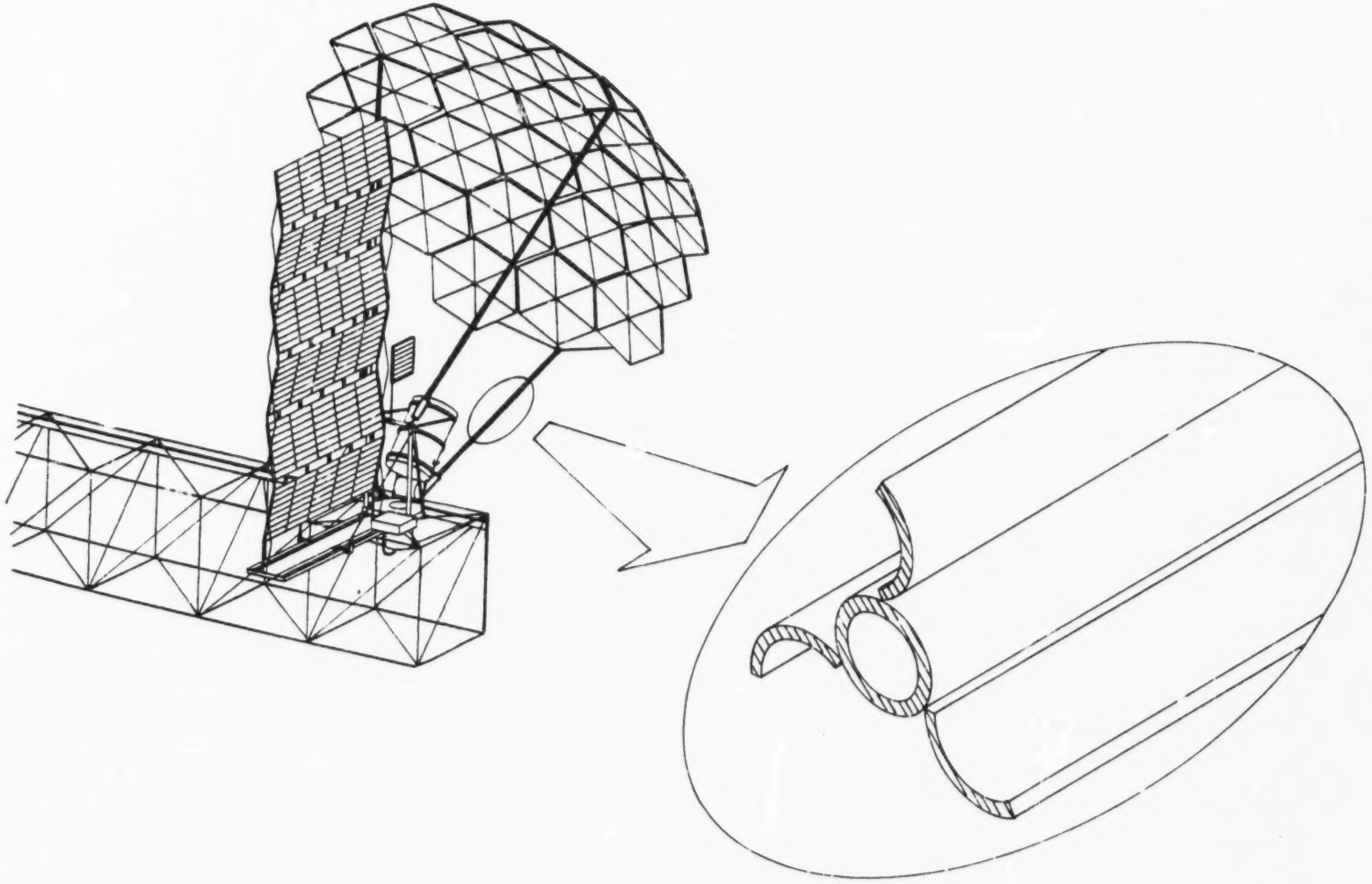

Figure 1. Fin-stiffened strut and large space structure application.

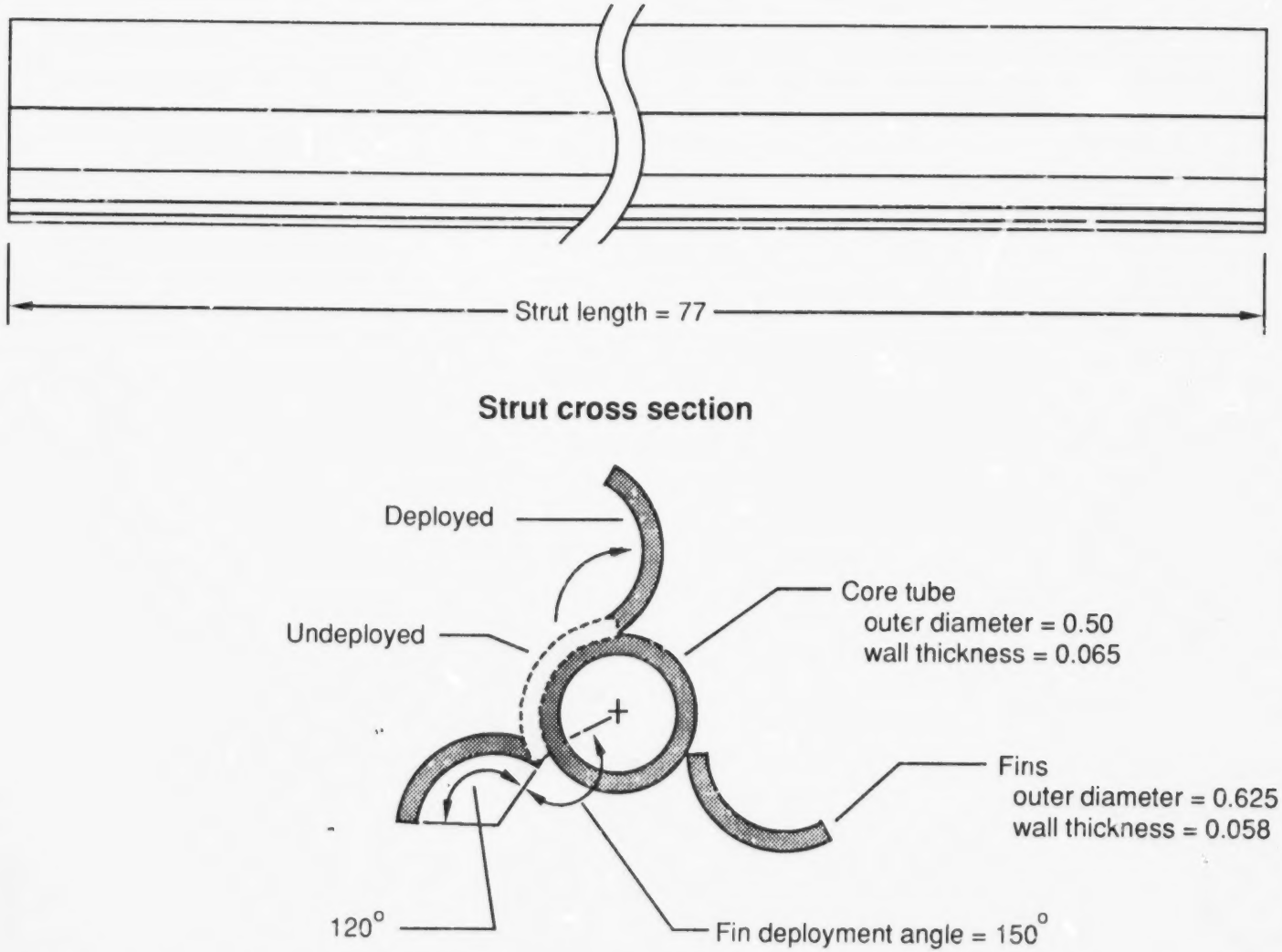

Figure 2. Fin-stiffened strut analysis and test configuration. Linear dimensions are in inches.

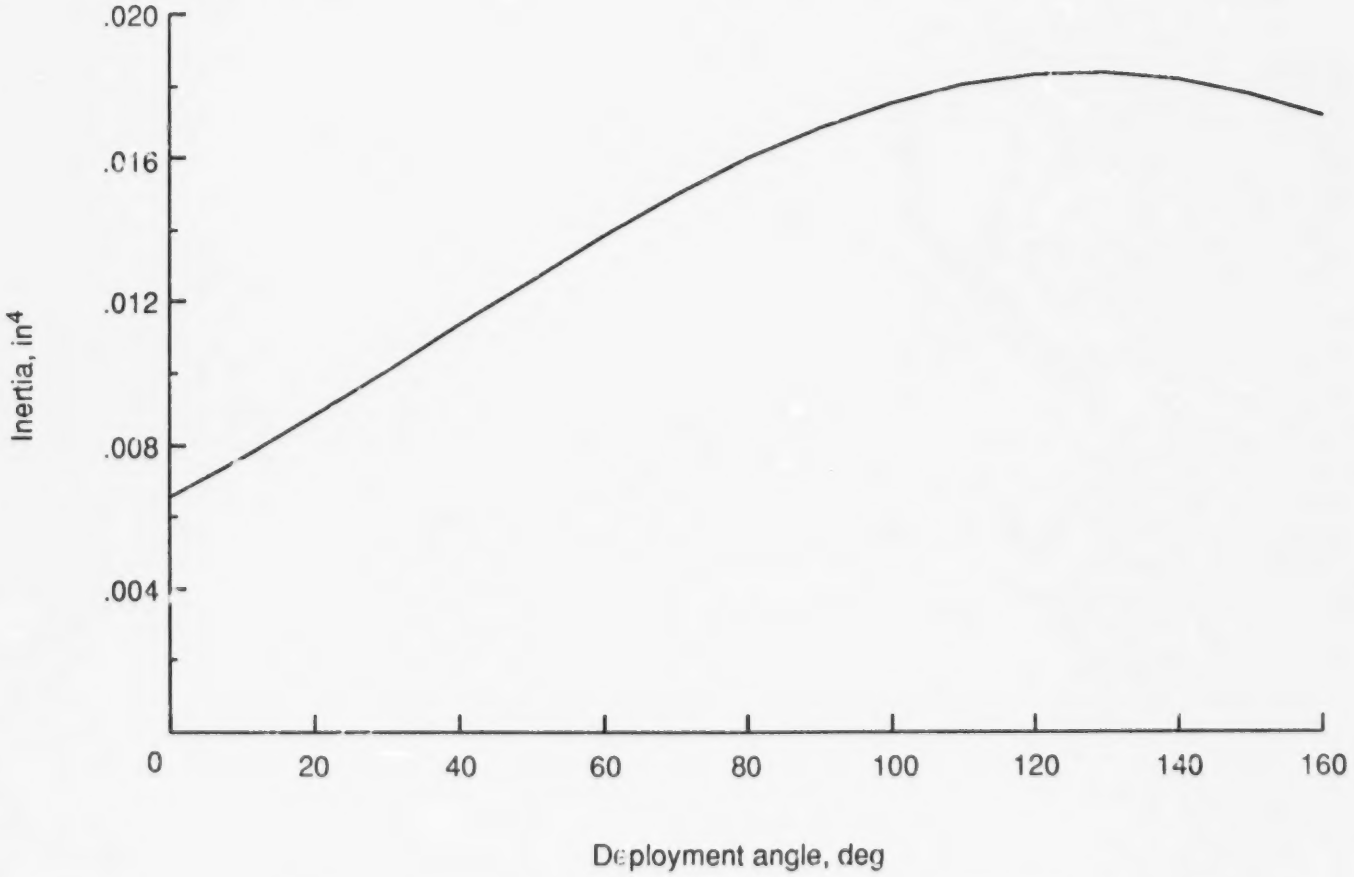

Figure 3. Variation of cross-sectional inertia with fin deployment angle.

ORIGINAL PAGE IS
OF POOR QUALITY

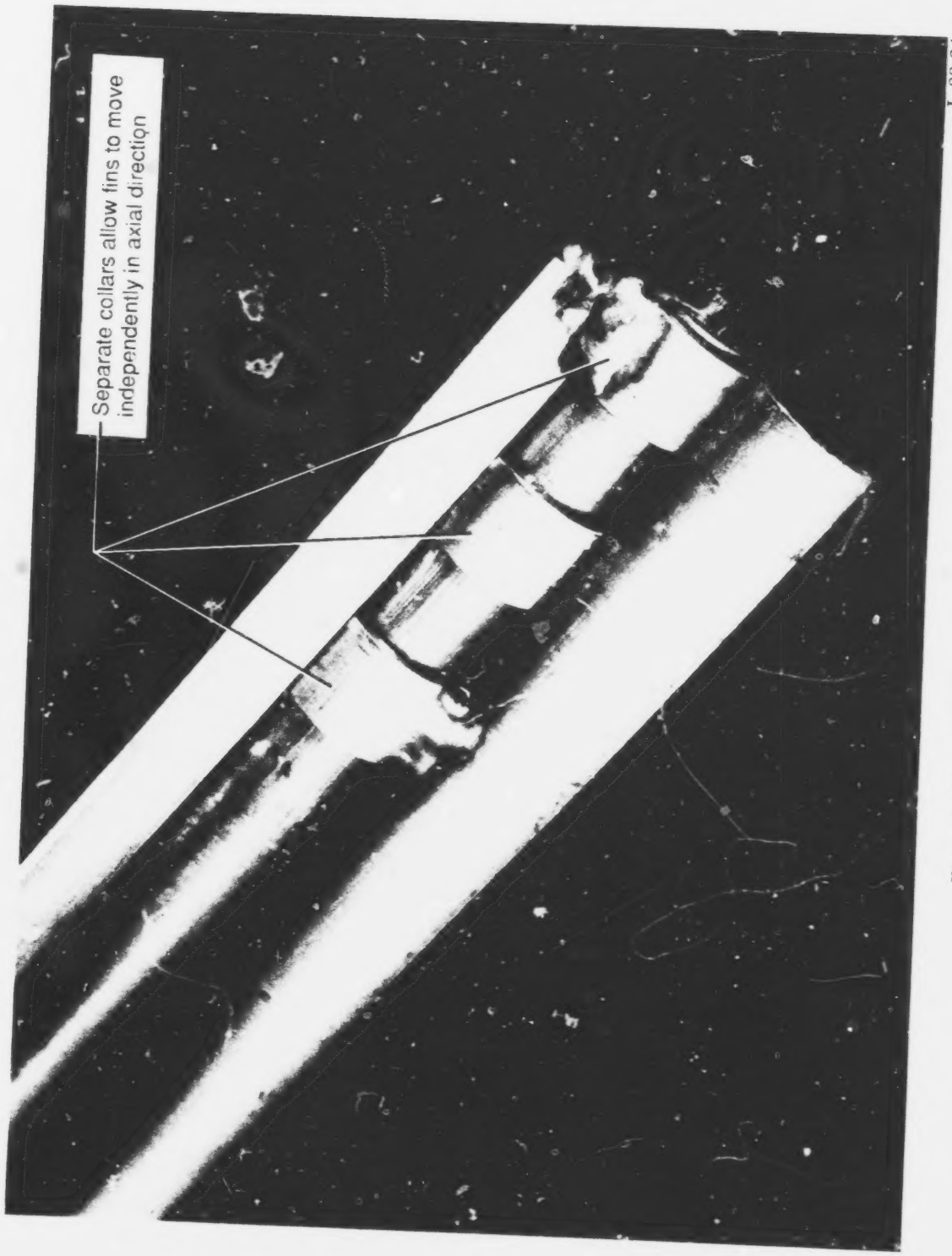

L-88-24

Figure 4. Fin attachment concept 1 (specimen 1).

ORIGINAL PAGE IS
OF POOR QUALITY

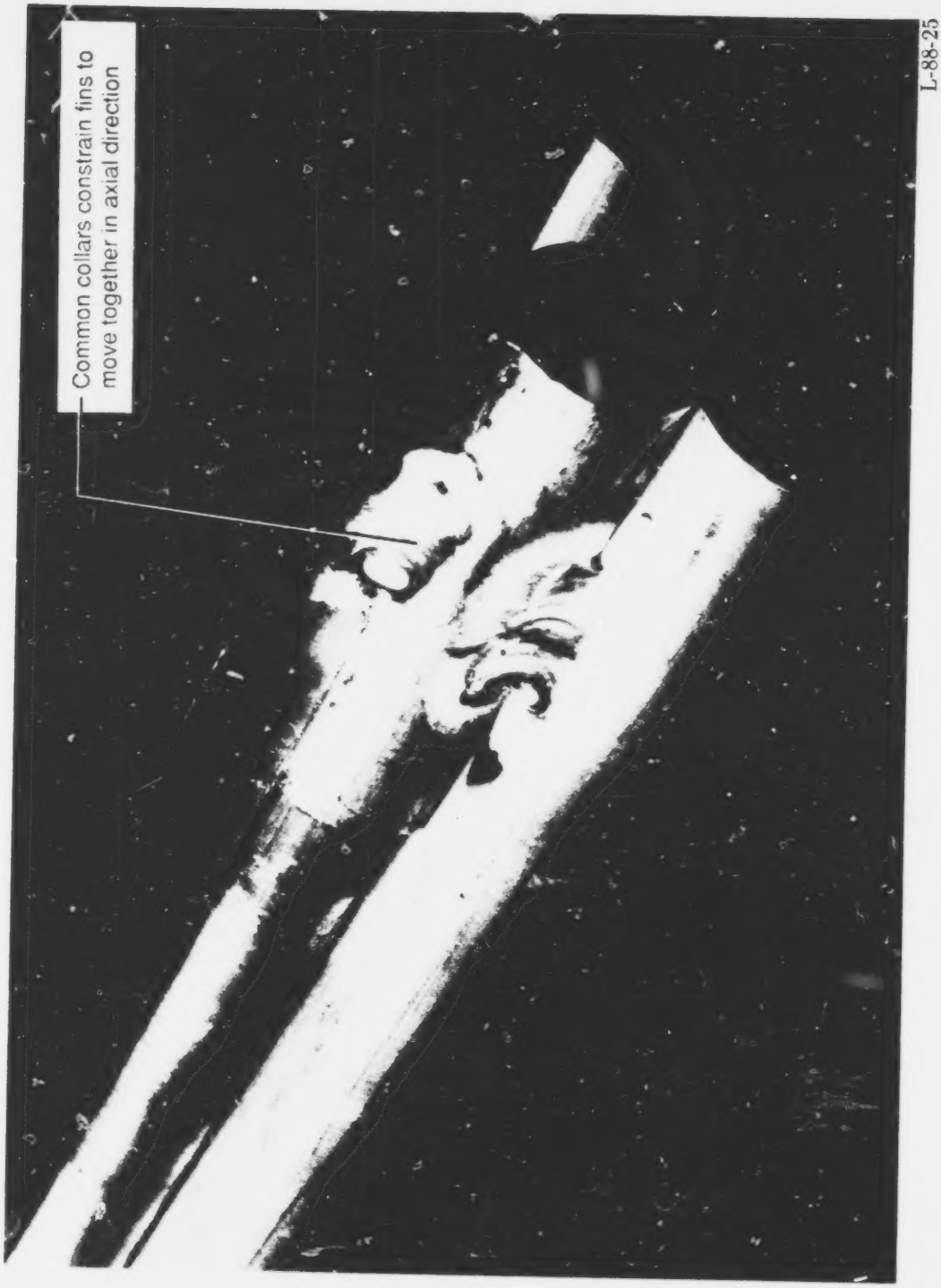

Figure 5. Fin attachment concept 2 (specimen 2).

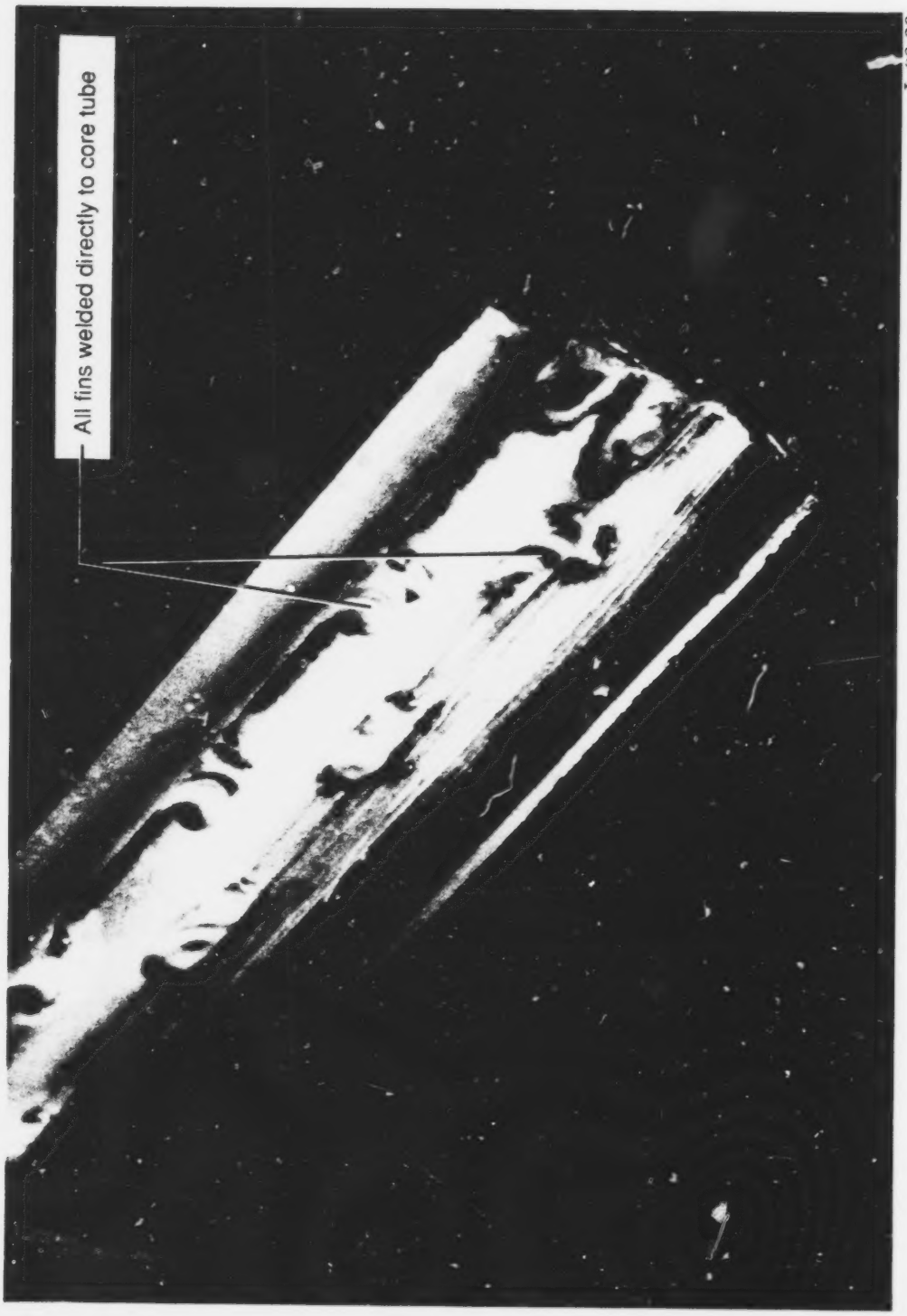

L-88-26

Figure 6. Fin attachment concept 3 (specimen 3).

ORIGINAL PAGE IS
OF POOR QUALITY

ORIGINAL PAGE IS
OF POOR QUALITY

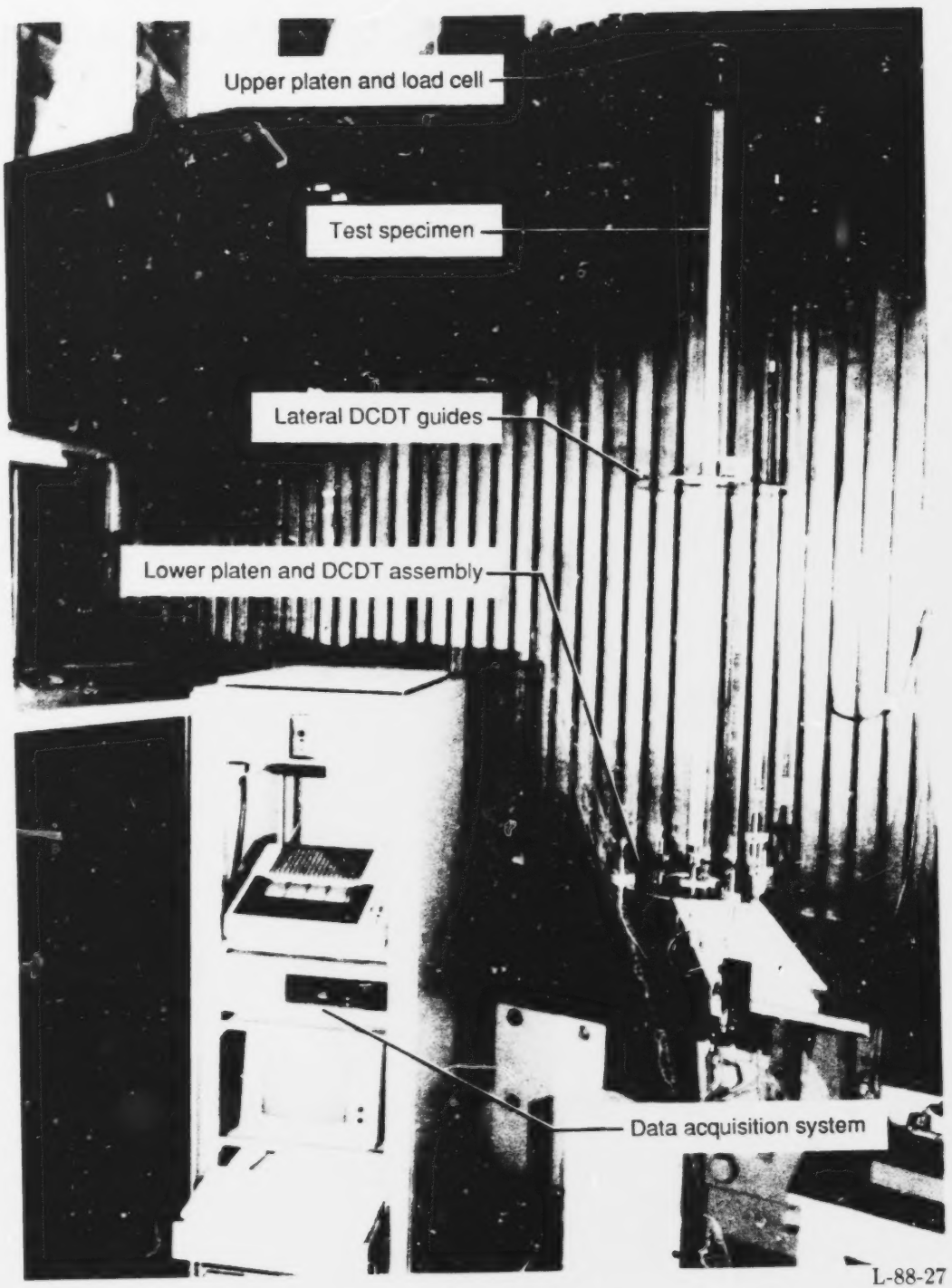

(a) Complete setup.

Figure 7. Experimental test setup.

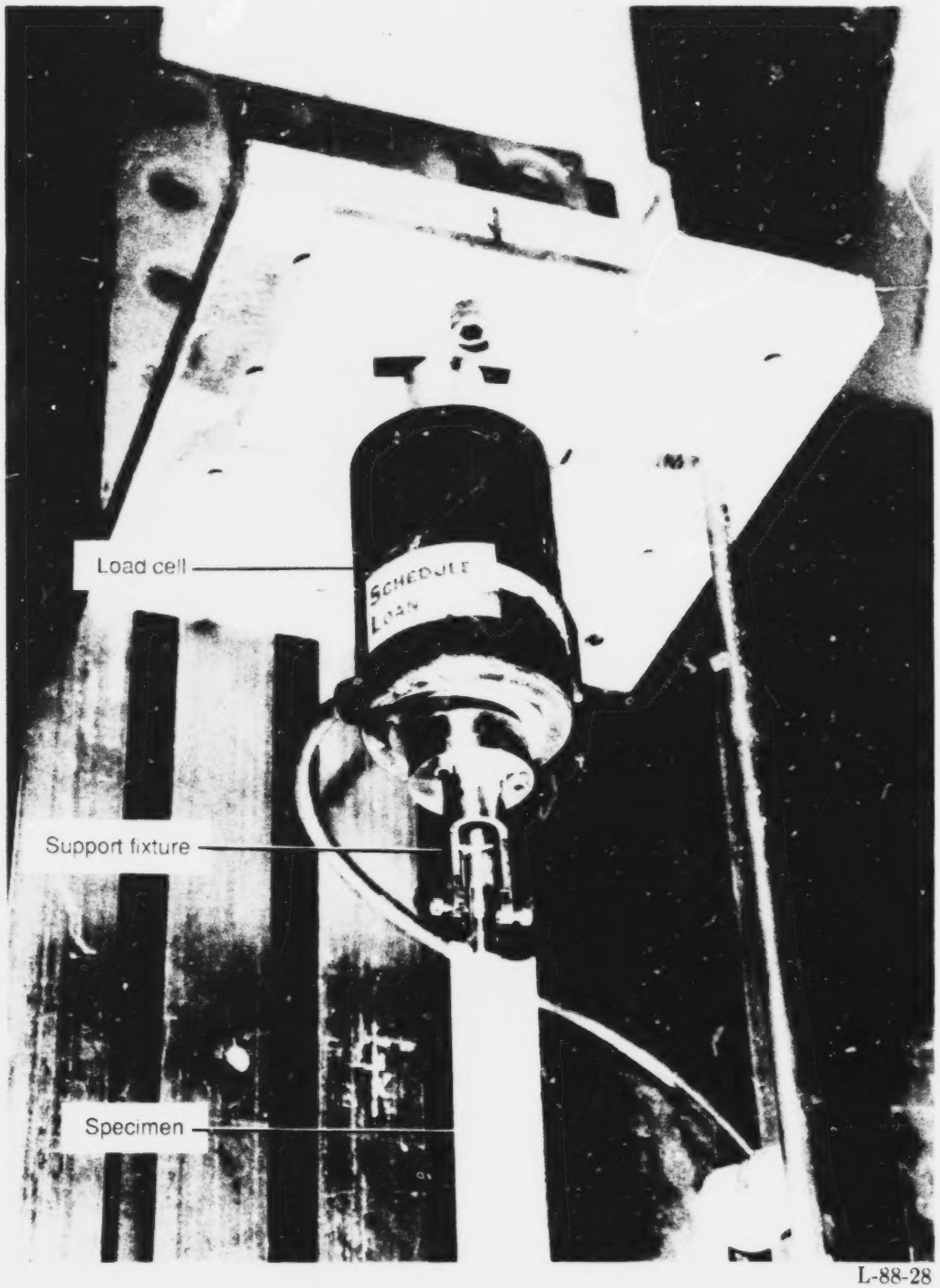

(b) Upper platen and load cell.

Figure 7. Continued.

ORIGINAL PAGE IS
OF POOR QUALITY

ORIGINAL PAGE IS
OF POOR QUALITY

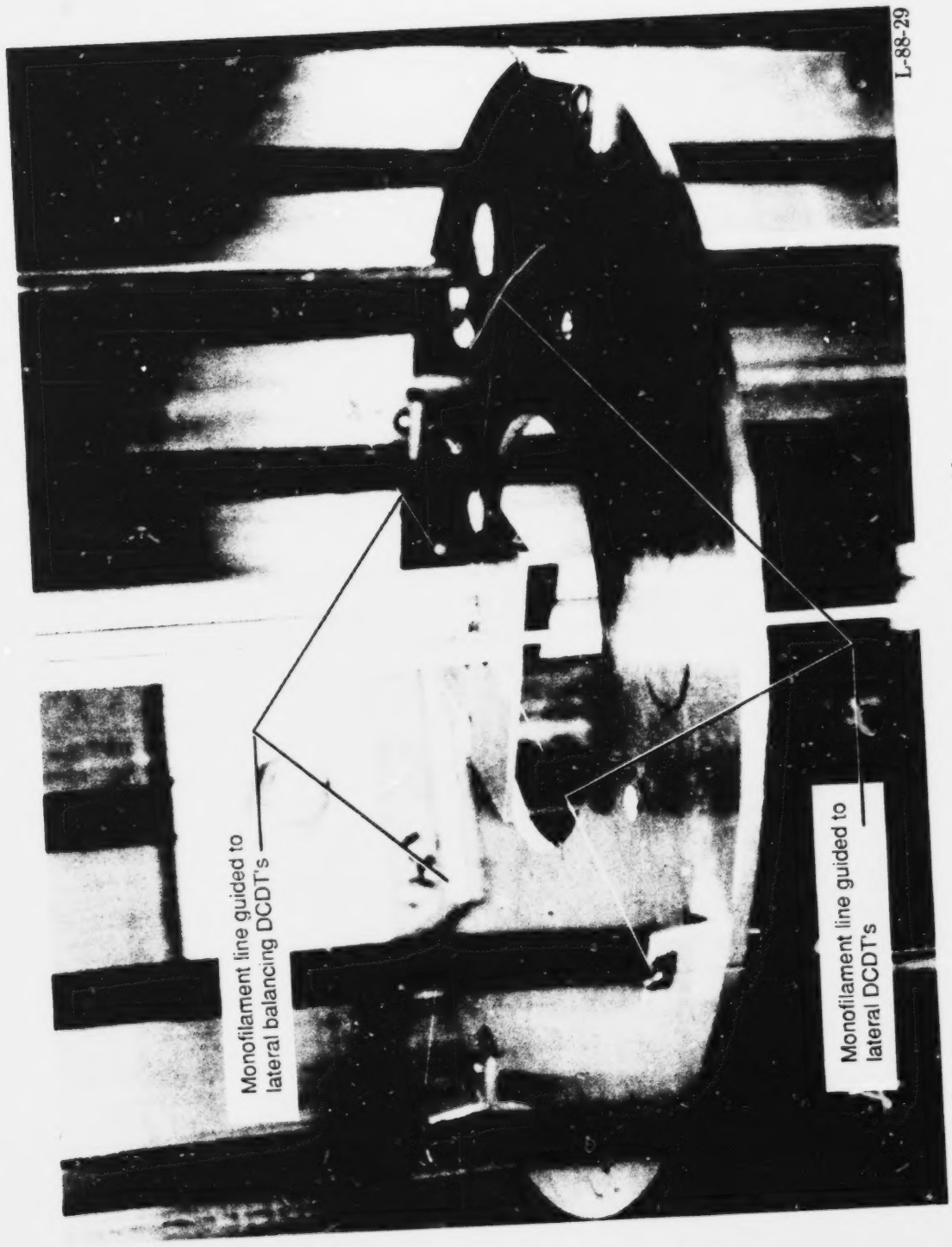

(c) Lateral DCDT guide assembly.

Figure 7. Continued.

ORIGINAL PAGE IS
OF POOR QUALITY

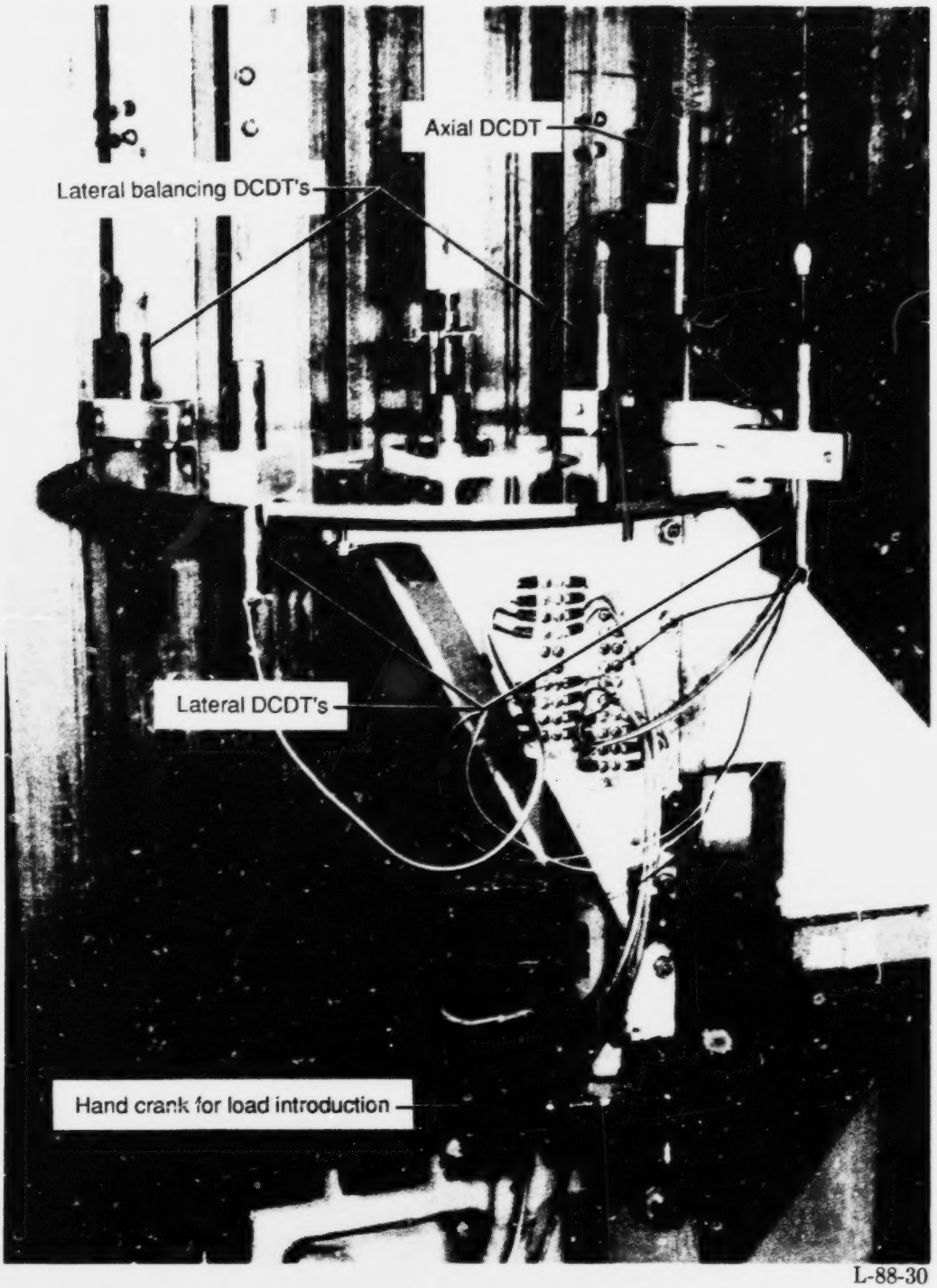

(d) Lower platen and DCDT assembly.

Figure 7. Concluded.

ORIGINAL PAGE IS
OF POOR QUALITY

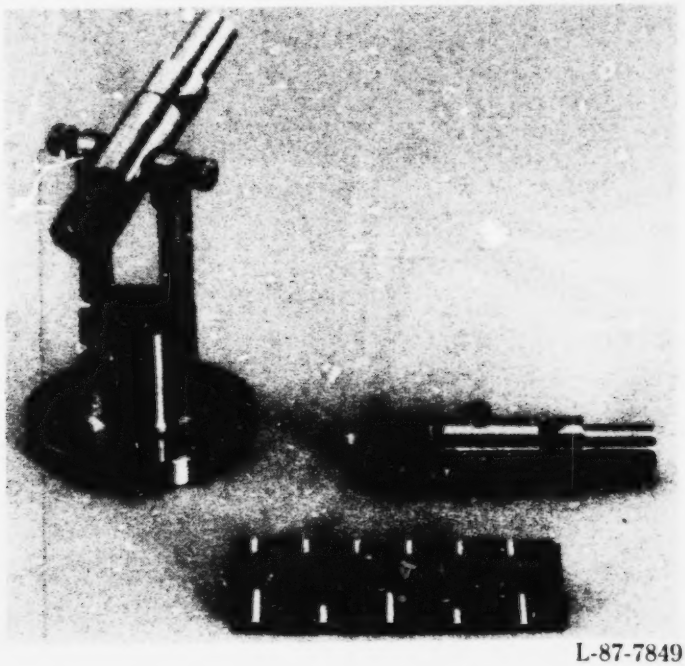

L-87-7849

(a) Pinned support fixture.

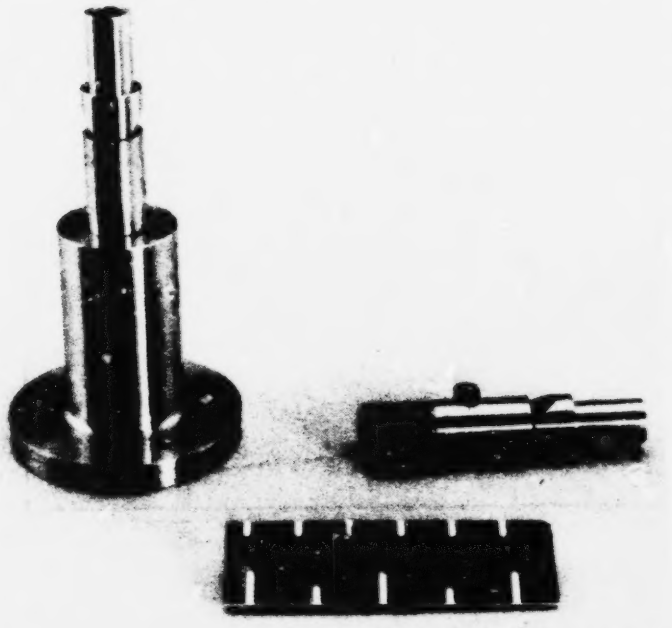

L-87-7850

(b) Partial restraint support fixture.

Figure 8. Support fixtures for ends of test specimens.

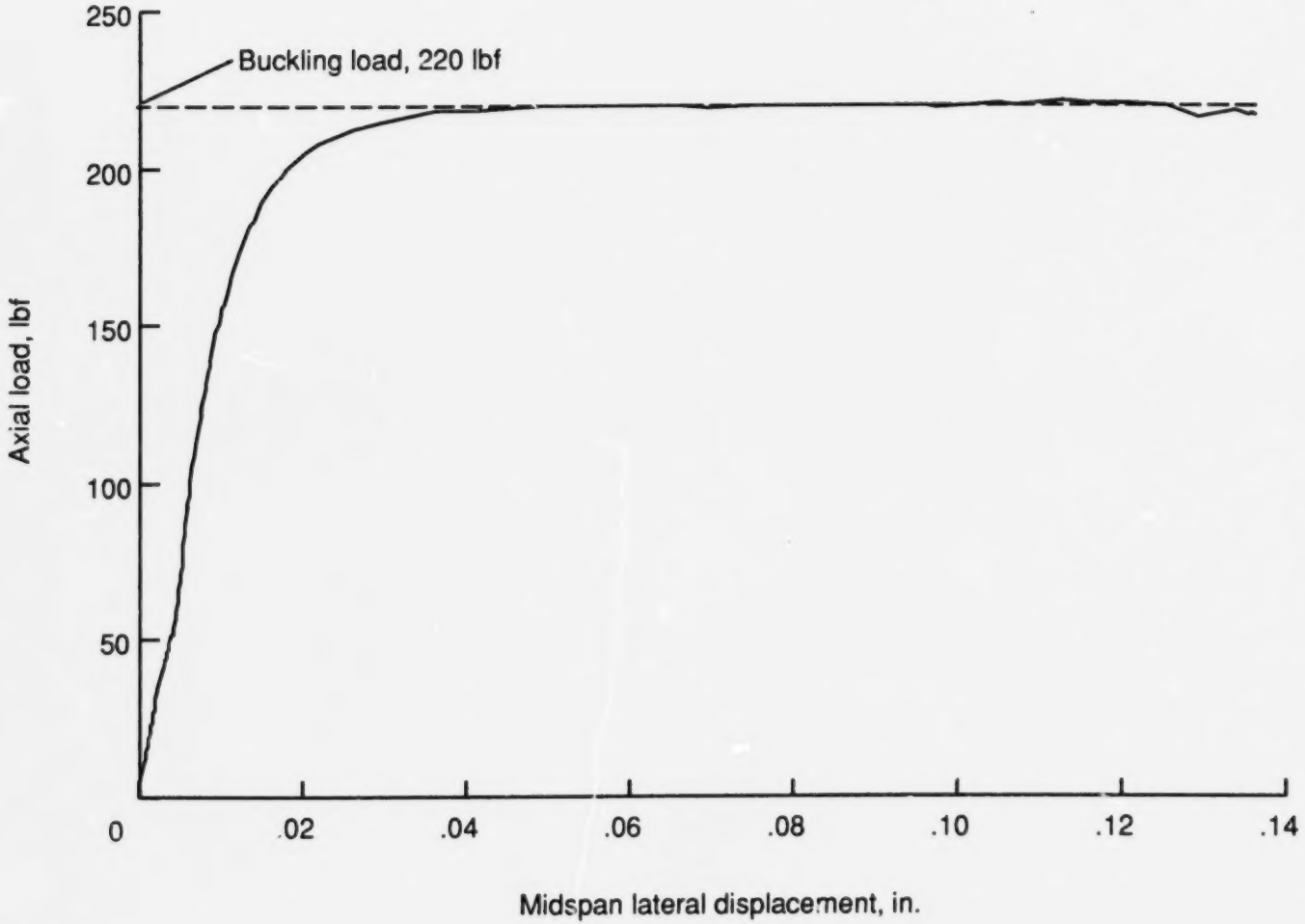

Figure 9. Typical plot of buckling load test data. Data from specimen 2, run 2.

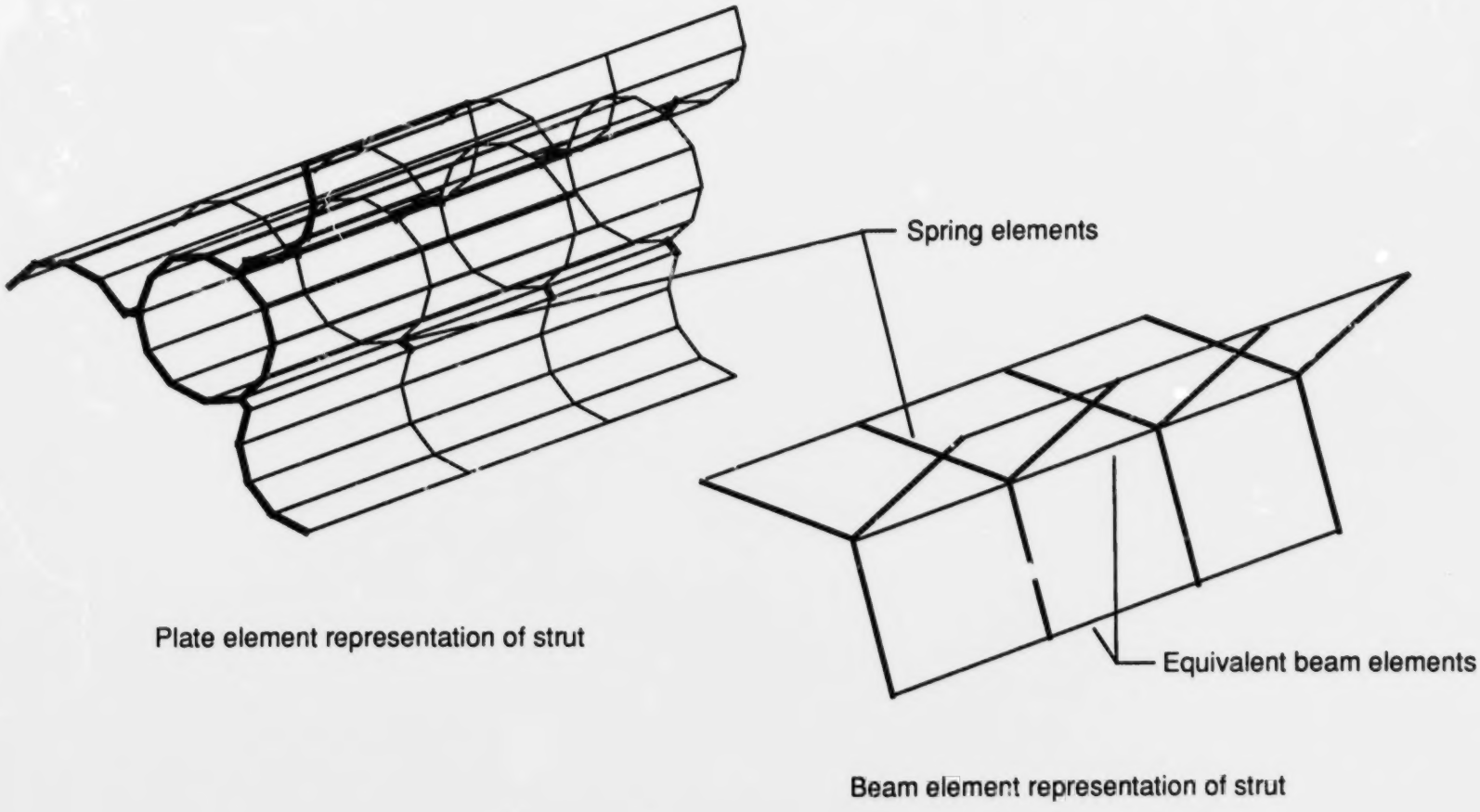

Figure 10. Finite element models of fin-stiffened strut.

NASA
National Aeronautics and Space Administration

Report Documentation Page

1. Report No.	2. Government Accession No.	3. Recipient's Catalog No.
NASA TM-4034		

4. Title and Subtitle	5. Report Date
Preliminary Investigation of Stability of a Fin-Stiffened Slender Strut	April 1988
	6. Performing Organization Code
7. Author(s)	8. Performing Organization Report No.
Mark S. Lake and K. Chauncey Wu	L-16411
9. Performing Organization Name and Address	10. Work Unit No.
NASA Langley Research Center Hampton, VA 23665-5225	506-43-41-02
	11. Contract or Grant No.
12. Sponsoring Agency Name and Address	13. Type of Report and Period Covered
National Aeronautics and Space Administration Washington, DC 20546-0001	Technical Memorandum
	14. Sponsoring Agency Code

15. Supplementary Notes

16. Abstract

A fin-stiffened strut concept which possesses high bending stiffness and low packaged volume has been identified for use on large space structures. The concept incorporates three curved fins which deploy from a core tube to increase the effective cross-sectional moment of inertia, the buckling load, and the vibration frequency of the strut. A strut design incorporating welded fin connections provides an upper bound of the strut buckling load. A strut design which allows the individual fins and core to move independently in the strut axial direction provides a lower bound of the strut buckling load which is approximately 20 to 25 percent of the upper bound. A practical strut design, incorporating hinge assemblies which constrain the fins to move together but independently of the core tube in the strut axial direction, provides a buckling load which is 75 to 80 percent of the upper bound. Euler's equation can be used to accurately predict buckling loads for the bounding designs. Flat plate finite element models of all designs give results that agree to within 10 percent of the experimental values. Equivalent beam models of the strut give results which are slightly less accurate.

17. Key Words (Suggested by Authors(s))	18. Distribution Statement
Buckling Stability Finite element analysis Fin-stiffened strut	Unclassified Unlimited Subject Category 18

19. Security Classif.(of this report)	20. Security Classif.(of this page)	21. No. of Pages	22. Price
Unclassified	Unclassified	22	A02

NASA-Langley, 1988
For sale by the National Technical Information Service, Springfield, Virginia 22161-2171